Mathematical Biosciences and Engineering

http://www.aimspress.com/journal/MBE

MBE, 18(6): 8641–8660.
DOI: 10.3934/mbe.2021428
Received: 08 July 2021
Accepted: 16 September 2021
Published: 09 October 2021

Research article

A mathematical model of drug dynamics in an electroporated tissue

Nilay Mondal [1,*], **Koyel Chakravarty**[2] **and D. C. Dalal**[1]

[1] Department of Mathematics, Indian Institute of Technology Guwahati, Guwahati, Assam 781039, India

[2] Department of Mathematics, Faculty of Science and Technology, ICFAI University Tripura, Tripura 799210, India

* **Correspondence:** Email: nilay.mondal@iitg.ac.in.

Abstract: In order to overcome the obstruction of cell membranes in the path of drug delivery to diseased cells, the applications of electric pulses of adequate potency are designated as electroporation. In the present study, a mathematical model of drug delivery into the electroporated tissue is advocated, which deals with both reversibly and irreversibly electroporated cells. This mathematical formulation is manifested through a set of differential equations, which are solved analytically, and numerically, according to the complexity, with a pertinent set of initial and boundary conditions. The time-dependent mass transfer coefficient in terms of pores is used to find the drug concentrations through reversibly and irreversibly electroporated cells as well as extracellular space. The effects of permeability of drug, electric field and pulse period on drug concentrations in extracellular and intracellular regions are discussed. The threshold value of an electric field ($E > 100$ V cm^{-1}) to initiate drug uptake is identified in this study. Special emphasis is also put on two cases of electroporation, drug dynamics during ongoing electroporation and drug dynamics after the electric pulse period is over. Furthermore, all the simulated results and graphical portrayals are discussed in detail to have a transparent vision in comprehending the underlying physical and physiological phenomena. This model could be useful to various clinical experiments for drug delivery in the targeted tissue by controlling the model parameters depending on the tissue condition.

Keywords: electroporation; drug delivery; reversibly and irreversibly electroporated cells; cell membrane; electric pulse

1. Introduction

One of the major difficulties in biotherapy and cancer chemotherapy is the paucity of potent drug and gene delivery. In order to deliver drug in the intracellular space, cell membrane acts as a barrier

and allows restrictive diffusion of drug molecules. Large size particles are almost impermeable through the membrane. Electroporation or electropermeabilization is used to increase the cell membrane permeability which is studied by many researchers [1–5]. Electroporation is a biophysical phenomenon resulting in the formation of aqueous pores in the cell membrane made of lipid bilayer. Electroporation is performed by applying an external electric field of sufficient strength [3, 5–7]. In electroporation, transmembrane potential increases with the application of electric field and once the transmembrane potential exceeds it's critical value, the cell membrane gets permeabilized [4, 8]. This permeabilized membrane is utilized to transport the drug into the intracellular space. Also, electroporation is widely used in biomedicine, biotechnology, food science & technology and environmental science [4, 5, 9].

Depending on the field strength and pulse duration, electroporation process can be categorized as reversible and irreversible electroporation. In reversible electroporation, the electric field is applied under a certain range so that the membrane is temporarily permeabilized and recover the original state spontaneously after removal of electric field [10]. Once the pulse period is over, the cell membrane starts closing its pores, which had opened due to the application of external electric field. This process is called membrane resealing [2, 11]. It has been observed that the time duration in pore creation is of the order of a microsecond whereas membrane resealing happens in the minute time scale [8, 12]. The reversibly electroporated cell undergoes the treatment, and once the pulse period is over, the cell membrane reseals. In irreversible electroporation, the electric field is applied high enough that leads to the permanent pore generation in the cell membrane [13]. The irreversible electroporation may lead to the loss in cell homeostasis that can lead to the cell death [14]. Thus, irreversibly electroporated cells can not sustain the treatment and pores do not reseal [15]. Reversible electroporation has been used to deliver drug into tumour cells through the process of electrochemotherapy [16, 17], gene delivery [18] and transdermal drug delivery [9, 19]. On the other hand, irreversible electroporation is generally used in cancer treatment [13, 14].

The efficacy of drug transport in the tissues, as an outcome of electroporation, depends on several electrical parameters, physical and biochemical properties of the tissue, and drug's physicochemical characterization. Electropermeabilization depends on pulse strength, pulse duration, and the number of pulses [20]. Some tissue properties such as conductivity, size, shape and distribution of cells also play a significant role in drug transport phenomena [12, 21]. Experimental findings reveal that the number of pulses and their duration are responsible for drug transport across the permeabilized membrane [22]. The application of a high voltage electric field for a short duration (1μs – $100\,\mu$s) increases pore density within the cell membrane in single cell electroporation [21,23]. However, in bulk electroporation, long-duration ($100\,\mu$s – 100 ms) electric pulses are generally conducted to electroporate the tissue [9,11,19].

Mathematical models are gradually taking the center stage in the research arena of drug delivery through electroporation. In 2008, Granot and Rubinsky [11] proposed a mathematical model of drug delivery in tissue cells with reversible electroporation. The authors used the model of single cell electroporation proposed by Krassowska and Filev [3] and described that the mass transfer rate in the cells is increased with pore creation due to electroporation. In 2014, the Miklavčič group [24] proposed a dual porosity model and established a relation between electroporation and the resulted permeability that affects macroscopic transport and cellular drug uptake. The dual porosity model is used to treat the biological materials with electroporation in food science [25]. The dual porosity model is also used in the study of Dermol-Černe et al. [17], which makes a connection between *in vitro* and *in vivo* experiments in electrochemotherapy. In a slightly different way, Boyd and Becker [26] presented

a model to implement tissue electroporation for drug delivery. The model considered the effects of tissue conductivity to increase cellular permeability in addition to the phenomenon of pore resealing. In 2017, Argus et al. [27] extended the said model including the transient transport behaviour of reversibly electroporated cells and that of irreversibly electroporated cells. In 2018, Dermol-Černe and Miklavčič [9] also developed a model of skin electroporation to study transdermal drug delivery through stratum corneum. The model described the changes in dielectric properties of the electroporated skin.

The present study deals with the mathematical modelling of tissue electroporation to introduce drug into the targeted cells. In this model, a uniform electric field is applied to electroporate the tissue; reversible as well as irreversible electroporation is considered, and membrane resealing effects are also taken into account. The principal purpose of this model is to have a detailed analysis of the drug transport through extracellular as well as intracellular region of the biological tissue. A time-variant mass transfer coefficient is considered to be dependent on membrane pore density as the increment of pores during electroporation enhances the drug transport into the cells. In this study, mass transfer during electroporation and after the termination of electroporation are investigated. The physical phenomena are demonstrated through a system of coupled differential equations along with appropriate initial and boundary conditions. Based on the mathematical complexities, some of the equations are solved analytically, and rest are solved numerically. The numerical scheme is validated by comparing the numerical results with analytical solutions. The effects of various significant parameters such as, field strength, pulse duration and drug permeability on transport phenomena, are discussed. It is found that a minimum electric field ($E > 100$ V cm^{-1}) is required to initiate the drug uptake into the cells. The local sensitivity analysis of various parameters of the model is also performed with graphical representations. A comparative study of the proposed model with the existing ones [11, 24, 26] is also carried out in order to have an idea about the potency and authenticity of the advocated model.

2. Problem formulation

In this work, a biological tissue is considered. The tissue is assumed to be spherical having radius R. From a macroscopic viewpoint, the tissue region may be categorically divided into two parts: extracellular space and intracellular space. The extracellular space is defined as the tissue region outside the cellular domain. The extracellular one is generally assumed to be outside the cell membrane, occupied by interstitial fluid and extracellular matrix. Intracellular space is a compartment within individual cells, as a whole, separated from the extracellular space by cell membranes. The cell membranes control the mass transfer of molecules, proteins, drugs etc., between extracellular and intracellular domains. The cell membrane contains millions of nanometre-sized pores through which drugs or some specific molecules may not be able to permeate. The complete structure of the biological tissue comprising of cells and porous cell membranes is schematically portrayed through Figure 1.

The fundamental aspect of tissue electroporation is that the cell membrane gets destabilized once electric pulses are applied [3,5]. Generally, electric pulses are used in two different approaches. Either a single pulse is applied continuously over a stipulated time period, or multiple pulses are applied for a time (pulse period) with some time gap between two pulses [5, 28]. During electroporation, cell membranes are permeabilized when the induced transmembrane potential exceeds its threshold value. In order to generate an electric field, two electrodes with different potential values ϕ_0, ϕ_L are placed at A and B respectively (as shown in Figure 2). A large number of hydrophilic transient pores are formed

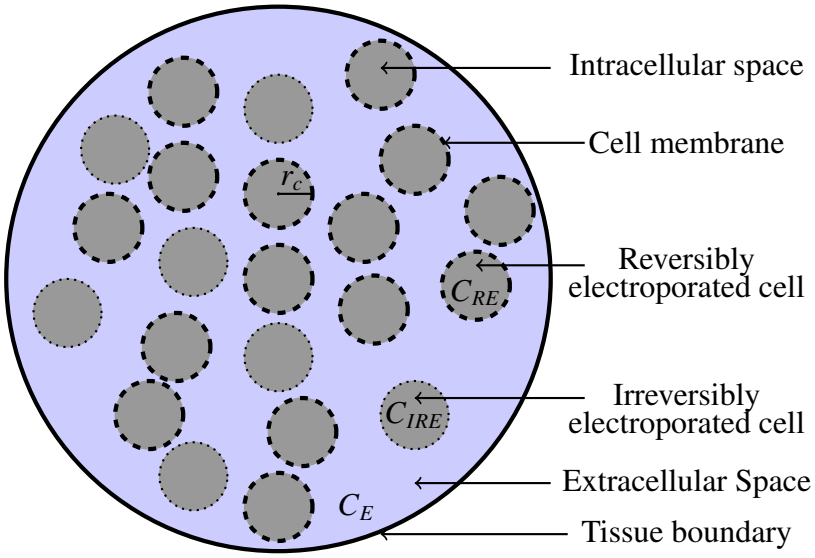

Figure 1. A schematic diagram of a biological tissue. Here, C_E: drug concentration in extracellular space; C_{RE}, C_{IRE}: drug concentrations in reversibly, irreversibly electroporated cells; r_c: cell radius.

due to electroporation so that the mass transport is expedited. In the present study, it is assumed that the pores are uniformly distributed in each cell surface, and the pore radius is considered to be constant for all cells embedded within the tissue. With the commencement of destabilization of the cell membrane, drug particles slowly move from the extracellular to the intracellular region. The number of pores per unit area on the cell surface increases in addition to the rise in the individual pore size, thus allowing enhanced drug uptake into the intracellular domain.

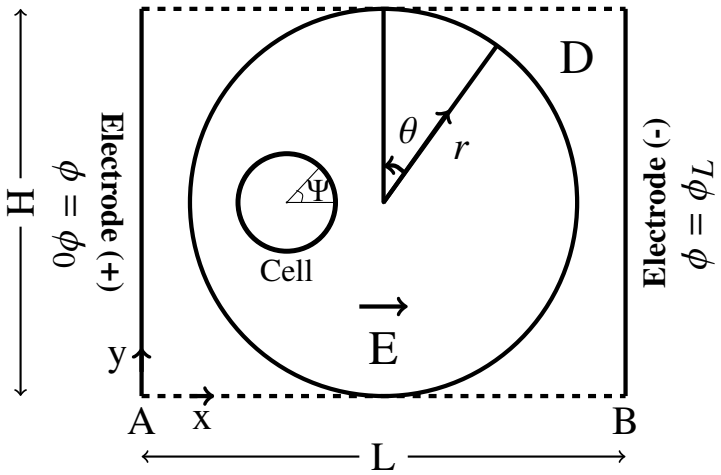

Figure 2. A schematic representation of bulk electroporation on a spherical tissue. Here L, H: length, width of the rectangular region D; ϕ_0, ϕ_L: electric potentials on the electrodes at A, B; E: induced electric field directed from left to right; r, θ: variables in spherical coordinates; ψ: angle between the direction of electric field and the normal to the cell membrane.

3. Model development

The biological tissue is usually represented as a conductive medium. Electroporation leads to augmentation of medium conductivity [8, 29]. The potential distribution, due to electroporation pulse induction, is obtained from the solution of Laplace equation. In order to mathematically model the electric field allied with electroporation, the Laplace equation is used [26] as follows,

$$\vec{\nabla} \cdot (\sigma \vec{\nabla} \phi) = 0, \tag{3.1}$$

where ϕ is the electrical potential, σ represents the extracellular conductivity and it is considered as constant. The boundary conditions are defined as $\phi = \phi_0$ on the electrode at A ($x = 0$) and $\phi = \phi_L$ on the electrode at B ($x = L$) (as shown in Figure 2. Value the electric field (E) is the magnitude of the gradient of the potential and is defined as $E = |\vec{\nabla}\phi|$.
The total number of pores (N_P) per cell surface (S) after the application of electric pulse is defined as

$$N_P(t) = \oint_S N(t)\, dS. \tag{3.2}$$

During electroporation, the pore density N in the cell membrane is evaluated by the equation, proposed in the model on single cell electroporation by Krassowka and Filev [3], which is as follows.

$$\frac{dN}{dt} = \alpha A \left[1 - \frac{N}{N_0} A^{-q}\right], \tag{3.3}$$

where $A = \exp\left[\left(\frac{V_m}{V_{ep}}\right)^2\right]$, t is the time, α is the pore creation rate coefficient, V_m is the transmembrane potential, V_{ep} is the characteristic voltage of electroporation, N_0 is the equilibrium pore density for the membrane area at $V_m = 0$ and q is an electroporation constant. The Eq (3.3) is derived from the two facts: (i) the pore creation rate depends on transmembrane potential exponentially and it agrees well with the experimental findings [30], (ii) Equation (3.3) is a stochastic description of pore creation and evolution, which is formulated from the Smoluchowki equation by Neu and Krassowska [31].
The transmembrane potential V_m, of a spherical cell in a uniform electrical field E was developed by DeBrurin and Krassowka [1] and is defined as,

$$V_m = 1.5E \times r_c \cos\Psi, \tag{3.4}$$

where r_c denotes the radius of the cell and Ψ is the angle between the direction of electric field and normal to the cell membrane at the position in which V_m is calculated.

In this model, the magnitude of the electric field is taken between 100 to 150 V cm^{-1}. Since the transmembrane potential reaches its peak at the poles $\Psi = 0$ and π, the maximum number of pores are created at those particular poles. Moreover, the transmembrane potential is almost null at $\Psi = \pi/2$ and $3\pi/2$ and therefore, no new pores are formed at those locations. The total area of pores (A_P) in the cell surface is calculated by the product of number of pores per cell and individual pore area and is represented mathematically as,

$$A_P = \pi R_P^2 \cdot N_P, \tag{3.5}$$

where R_P is the radius of a typical pore in the electroporated cell membrane. As already mentioned, Argus et al. [27] presented a mathematical model for tissue electroporation considering both reversible and irreversible electroporation. In their work, two different mass transfer coefficients were considered for reversibly and irreversibly electroporated cells in the mass transport equations. In the present study, a more generalised mass transfer coefficient, which is considered to be dependent on the total number of pores, is used. The mathematical formulation of the mass transfer coefficient μ ($\sec^{-1}$), which is applicable to both reversibly and irreversibly electroporated cells, is given as follows,

$$\mu(t) = \left(\frac{\pi R_P^2}{V_0}\right) \cdot N_P(t) \cdot P, \tag{3.6}$$

where V_0 is the volume of a cube that just contains a cell and P is the permeability of drug particles across the cell membrane.

In this investigation, the following two cases are studied:

3.1. Case 1: Mass transfer during ongoing electroporation

In the present case, it is assumed that the drug is injected prior to the initiation of the electroporation process. Furthermore, it is considered that a uniform electric field is applied continuously for a particular time duration so that the drug particles get transported into the intracellular compartment from the extracellular one, once the cell membrane starts destabilizing. The electric pulses are applied continuously on the tissue throughout the process of drug diffusion from the extracellular to intracellular domain. The electric pulses are halted on the completion of the drug diffusion phenomenon. Hence, no resealing effect is observed during this molecular diffusion since the time duration required for resealing effect is not achieved by the membrane pores of reversibly electroporated cells. Thus, the increased pore area obtained from the Eq (3.5) remains constant with time. For the present case, the mass transfer coefficient is considered to be the same as given in the Eq (3.6). The extracellular space can be thought of as the temporary reservoir of the drug, and the present investigation focuses on how the drug is being transported into the reversibly and irreversibly electroporated cells from the extracellular region when the electroporation process is on. Accordingly, the drug dynamics, during ongoing electroporation, is manifested through the subsequent mathematical formulation [27] as,

$$\frac{\partial C_E}{\partial t} = \vec{\nabla}.\left(D_{eff}\vec{\nabla}C_E\right) - \left(\frac{1-\varepsilon}{\varepsilon}\right)\mu(t) \times \left[SF\,(C_E - C_{RE}) + (1 - SF)(C_E - C_{IRE})\right], \tag{3.7}$$

with initial condition: $C_E(r, \theta, 0) = C_0$,
where C_E is the drug concentration in the extracellular space, C_{RE} and C_{IRE} are the drug concentrations in the reversible and irreversible electroporated cells respectively, C_0 is the initial drug concentration in the extracellular domain, D_{eff} is the effective diffusion coefficient of the drug in the extracellular space, ε is the porosity (i.e., the volumetric ratio between extracellular volume and total volume), and SF is the survival fraction of cells. In Eq (3.7), the left hand side represents the rate of change of drug concentration with time in extracellular space, the first term in the right hand side represents drug diffusion in the extracellular media and the second term (as reaction) represents the total amount of mass transfer at time t from extracellular into intracellular domain with mass transfer coefficient $\mu(t)$ (see Eq (3.6)).

The governing equations for the drug dynamics in the reversibly and irreversibly electroporated cells can be written as,

$$\frac{\partial C_{RE}}{\partial t} = \mu(t) \cdot (C_E - C_{RE}), \tag{3.8}$$

$$\frac{\partial C_{IRE}}{\partial t} = \mu(t) \cdot (C_E - C_{IRE}), \tag{3.9}$$

with initial conditions:
$C_{RE}(r, \theta, 0) = 0$, $C_{IRE}(r, \theta, 0) = 0$.

Equations (3.8) and (3.9), which come from the mass balance equation, represent the rate of drug uptake into the reversibly and irreversibly electroporated cells. Since, a uniform electric field is applied during electroporation, the whole tissue is electroporated uniformly. Mass transport from extracellular space into intracellular space occurs through molecular diffusion due to concentration gradient. Since, initially the concentrations in extracellular ($C_E = C_0$) and intracellular ($C_{RE} = 0$, $C_{IRE} = 0$) regions are different, mass transport continues to occur until the concentrations becomes equal (i.e., $C_E = C_{RE} = C_{IRE}$). The concentration variables may be considered as space independent due to uniform electroporation and homogeneous media. Hence, only temporal changes in drug concentrations are emphasized here. On considering $\nabla^2 C_E = 0$ and D_{eff} as constant, the Eqs (3.7) – (3.9) are simplified as,

$$\frac{dC_E}{dt} = -\left(\frac{1-\varepsilon}{\varepsilon}\right)\mu(t) \times [SF \cdot (C_E - C_{RE}) + (1 - SF) \cdot (C_E - C_{IRE})], \tag{3.10}$$

$$\frac{dC_{RE}}{dt} = \mu(t) \cdot (C_E - C_{RE}), \tag{3.11}$$

$$\frac{dC_{IRE}}{dt} = \mu(t) \cdot (C_E - C_{IRE}), \tag{3.12}$$

subject to initial conditions:
$C_E(0) = C_0$, $C_{RE}(0) = C_{IRE}(0) = 0$.

3.2. Case 2: Mass transfer after the termination of electroporation

In this case, the drug is assumed to be injected into the biological tissue immediately after the electroporation process is stopped. Moreover, it is considered that continuous electroporation is actioned due to the application of a uniform electric field for a specific time span t_{ep}. Before the initiation of electroporation, there is no accumulation of the drug in the extracellular space, whereas drug transport into the intracellular compartment starts immediately after the end of the pulse period. At this juncture, as the reversibly electroporated cell membrane pores get adequate time to reseal, the pore area starts decreasing with time. Hence, the pore area can be mathematically illustrated through an exponentially decreasing function of time [11], which is as follows.

$$A_P = \pi R_P^2 \cdot N_P \cdot \exp\left(-\frac{t}{\tau}\right), \tag{3.13}$$

where τ is the resealing time constant.

In this case, we take $\mu(t_{ep}) = \left(\frac{\pi R_P^2}{V_0}\right) \cdot N_P(t_{ep}) \cdot P$, which represents the mass transfer coefficient and the Eqs (3.10)–(3.12) are remodelled as Eqs (3.14)–(3.16) respectively,

$$\frac{dC_E}{dt} = -\left(\frac{1-\varepsilon}{\varepsilon}\right)\mu(t_{ep}) \times \left[\exp\left(-\frac{t}{\tau}\right) \cdot SF \cdot (C_E - C_{RE}) + (1 - SF) \cdot (C_E - C_{IRE})\right], \tag{3.14}$$

$$\frac{dC_{RE}}{dt} = \mu(t_{ep}) \cdot \exp\left(-\frac{t}{\tau}\right) \cdot (C_E - C_{RE}), \tag{3.15}$$

$$\frac{dC_{IRE}}{dt} = \mu(t_{ep}) \cdot (C_E - C_{IRE}), \tag{3.16}$$

with initial conditions:
$C_E(0) = C_0$, $C_{RE}(0) = C_{IRE}(0) = 0$.

4. Methods of solution

In this model, both analytical and numerical methods are applied to solve the governing equations wherever applicable. The Eq (3.1) is solved analytically in the rectangular region D ($0 \le x \le L$, $0 \le y \le H$). It is observed from the geometry (Figure 2) that ϕ is independent of y and $\frac{\partial \phi}{\partial y} = 0$. Equations (3.2) and (3.3) are also solved analytically considering $\Psi = 0$ or π. The coupled Eqs (3.10)–(3.12) are solved analytically and also numerically using the finite difference method. A comparison between analytical and numerical results is conducted to ensure the accuracy of the numerical scheme. This validation is required as the same numerical scheme is used to solve the coupled Eqs (3.14)–(3.16). For this purpose, Euler explicit method is used with a time step $\Delta t = 10^{-5}$ sec. The parameter values used in the present work are provided in Table 1. Solutions are obtained for various parameter values, and computations are performed in a computer having an Intel-core i5 processor and 4GB RAM. Plots of numerical solutions are obtained with the help of Matlab R2019a.

4.1. Analytical solutions

The potential function $\phi(x)$ is obtained from Eq (3.1) with the specified boundary conditions as

$$\phi(x) = \frac{(\phi_L - \phi_0)}{L}x + \phi_0. \tag{4.1}$$

The uniform electric field in the whole region D is

$$E = \frac{(\phi_0 - \phi_L)}{L}. \tag{4.2}$$

Solving the Eq (3.3) with initial condition $N(0) = 0$, the pore density $N(t)$ is

$$N(t) = N_0 A^q \left[1 - \exp\left(-\frac{\alpha t}{N_0 \cdot A^{q-1}}\right)\right]. \tag{4.3}$$

The total number of pores on a cell surface (S) is obtained from the Eq (3.2) as

$$N_P(t) = 4\pi r_c^2 \cdot N(t). \tag{4.4}$$

Table 1. Parameter values used for simulation of the model.

Sym	Value	Definition(Source)
σ	0.241 S m^{-1}	Extracellular conductivity [27]
r_c	5×10^{-5} m	Cell radius [3]
α	10^9 m $^{-2} sec^{-1}$	Pore creation coefficient [3]
V_{ep}	0.258 V	Characteristic voltage [3]
N_0	1.5×10^9 m^{-2}	Equilibrium pore density [3]
q	2.46	Electroporation constant [11]
D_{eff}	10^{-11} m^2 sec^{-1}	Effective diffusion coefficient
R_P	0.8×10^{-9} m	Pore radius [11]
ε	0.18	Porosity (volumetric ratio) [24, 27]
P	5×10^{-7} m sec^{-1}	Permeability of drug [11]
SF	0.8	Survival fraction of cells [27]
τ	100 sec	Resealing time constant [27]
E	140 V cm^{-1}	Electrical field
C_0	10^{-6} mol L^{-1} = 10^{-6} M	Initial drug concentration
t_{ep}	20 sec	Time duration of electroporation
L	2.5×10^{-3} m	Length of the rectangle (Figure 2)
H	2×10^{-3} m	Width of the rectangle (Figure 2)
R	1×10^{-3} m	Radius of the tissue (Figure 2)
ϕ_0	35 V	Potential at A (Figure 2)
ϕ_L	0 V	Potential at B (Figure 2)
f_p	1.4×10^{-5}	Pore surface fraction ratio [24, 32]
d_m	5×10^{-9} m	Cell membrane thickness [24]

Using Eqs (3.11) and (3.12) in Eq (3.10), it becomes

$$\frac{dC_E}{dt} = -\left(\frac{1-\varepsilon}{\varepsilon}\right) \times \left[SF \cdot \frac{dC_{RE}}{dt} + (1-SF) \cdot \frac{dC_{IRE}}{dt}\right]. \tag{4.5}$$

Now, integrating the Eq (4.5) and using the initial conditions, C_E can be expressed as,

$$C_E = C_0 - \left(\frac{1-\varepsilon}{\varepsilon}\right) \times \left[SF \cdot C_{RE} + (1-SF) \cdot C_{IRE}\right]. \tag{4.6}$$

From Eqs (3.11) and (3.12), we have

$$\frac{d}{dt}(C_{RE} - C_{IRE}) = -\mu(t) \cdot (C_{RE} - C_{IRE}). \tag{4.7}$$

Integrating the Eq (4.7) and using the initial conditions, a relation between C_{RE} and C_{IRE} can be obtained as,

$$C_{RE} = C_{IRE}. \tag{4.8}$$

By substitutig C_E from the Eq (4.6) into the Eq (3.11), we have

$$\frac{dC_{RE}}{dt} = \mu(t) \cdot \frac{C_0\varepsilon - C_{RE}}{\varepsilon}. \tag{4.9}$$

Substitutig $\mu(t)$ into the above equation, we obtained C_{RE} and C_{IRE} as,

$$C_{IRE}(t) = C_{RE}(t) = C_0\varepsilon \times \left[1 - \exp\left(\frac{k_1}{k_2\varepsilon} \cdot \{1 - k_2 t - \exp(-k_2 t)\}\right)\right], \tag{4.10}$$

where $k_1 = \frac{\pi^2 R_P^2 N_0 P A^q}{2r_c}$ and $k_2 = \frac{\alpha}{N_0 A^{q-1}}$.
Finally, from the Eq (4.6), C_E can be obtained as,

$$C_E(t) = C_0\left[\varepsilon + (1-\varepsilon) \times \exp\left(\frac{k_1}{k_2\varepsilon} \cdot \{1 - k_2 t - \exp(-k_2 t)\}\right)\right]. \tag{4.11}$$

5. Results and discussion

The objective of the current study is to characterize the drug transport kinetics in the biological tissue. This characterization is done through qualitative analysis that can be visualized from Figures 3–13. The detailed qualitative analysis through the graphical representations reveal the underlying physical and physiological phenomena. Arbitrary choice of parameter values may not lead to the projected objectives of the present study. Hence, extensive literature is consulted, and model parameter values are obtained from the relevant literature and presented in Table 1. In this section, a detailed discussion on the effects of various model parameters, like drug permeability (P), electric field (E) and pulse duration (t_{ep}) is presented. Since the drug concentrations in different regions are space independent, the graphs (Figures 4–13) are plotted for a typical location. Figure 3 shows the semilog

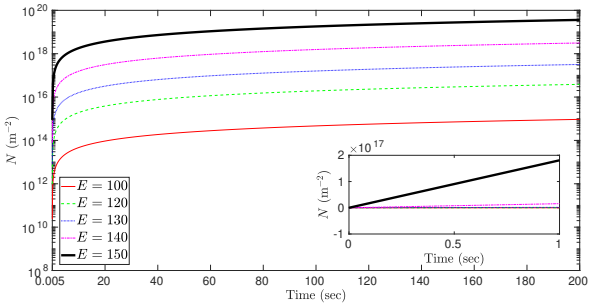

Figure 3. Represents the change of pore density N (m^{-2}) with time t for different electrical fields E (V cm^{-1}). This is a semilog plot for better understanding of the changes of N. The normal plot is shown in the inset for initial 1 sec.

plot for N against t to accommodate the wide range of variations in N. As initially ($t = 0$), the pore density is zero ($N = 0$), so log N is not defined at the initial time. In order to avoid this, we have plotted from $t = 0.005$ instead of $t = 0$. However, to verify the initial condition, we have shown the actual plots for the initial time, in the inset. This figure depicts the time variant pore density (N) change with the application of different electric fields. It may be observed from the figure that with the increasing electric field, the pore density increases. This is a very usual phenomena as the electroporation itself is dependent on the above mentioned electrical parameters.

5.1. Validation of the results

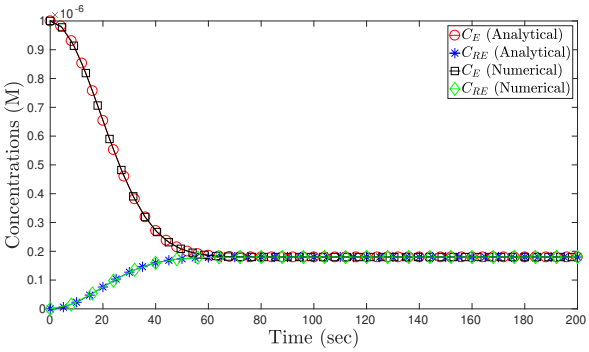

Figure 4. A comparison between the analytical and numerical results of drug concentrations C_E and C_{RE} (or C_{IRE}) for the case 1 (Mass transfer during ongoing electroporation) is shown. Here, analytical results corresponding to the Eqs (4.10), (4.11) and numerical results of the Eqs (3.10)–(3.12) for $P = 5 \times 10^{-7}$ m sec^{-1}, $E = 140$ V cm^{-1} are plotted.

In order to validate the numerical scheme of this model, a comparison between numerical and analytical solutions of drug concentrations in extracellular and intracellular regions is done as shown in the Figure 4. From the figure, it is seen that both the profiles of analytical and numerical results agree perfectly for each of the cases of C_E and C_{RE}. This computational scheme is used to solve the Eqs (3.14)–(3.16).

5.2. Mass transfer during ongoing electroporation

In this section, it is considered that the drug is transported from extracellular space into the intracellular space when the electroporation process is under way. It may be kept in mind that the resealing effect is not significant in this phase, as discussed earlier.

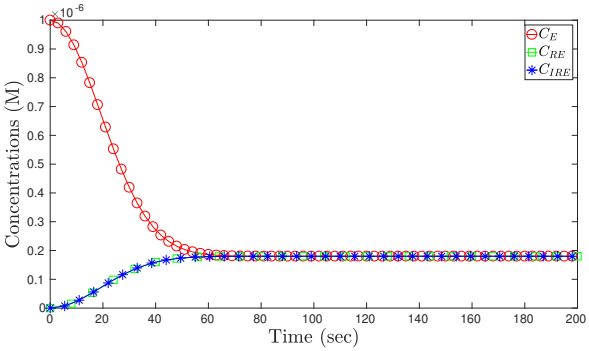

Figure 5. Time variant drug concentration profiles of C_E, C_{RE} and C_{IRE} for $P = 5 \times 10^{-7}$ m sec^{-1} and $E = 140$ V cm^{-1}.

Figure 5 represents the time variant concentration profiles of drug concentrations in extracellular space, reversibly and irreversibly electroporated cells, respectively. In the present scenario, electroporation and resultant mass transfer, i.e., drug transport in particular, are in simultaneous action so that there is no time for resealing effect. These events can be clearly visualized from Figure 5. As the

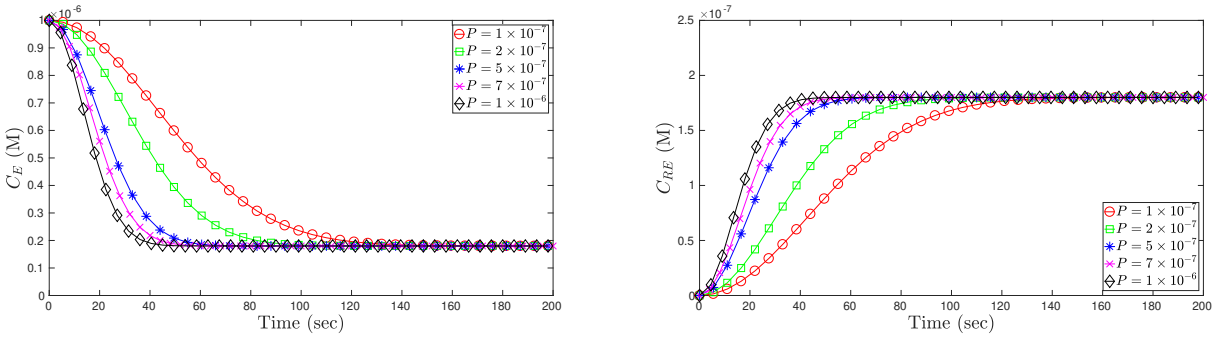

(a) **(b)**

Figure 6. Time variant drug concentration profiles of (a) C_E and (b) C_{RE} (or C_{IRE}) for different P (m sec^{-1}) and $E = 140$ V cm^{-1}. The drug concentrations (C_{RE}, C_{IRE}) are exactly same as there is no resealing effect.

drug has its maximum concentration in the extracellular space, its contour declines from the peak once the drug starts entering into the intracellular space. On the other hand, the drug concentrations in reversibly and irreversibly electroporated cells increase from their initial zero concentrations due to drug uptake. Moreover, due to insignificant resealing effect, the reversibly and irreversibly electroporated cells behave similarly, and hence their corresponding contours overlap, which is evident from the figure itself. In the mathematical formulation, the physiological processes starting form electroporation upto drug uptake by the cells are considered. Here, any mode of drug clearance or drug degradation is not modeled. Thus, the residual drug accumulates in the extracellular space due to the absence of drug clearance. The maximum limit of drug uptake is attained by the cells before drug degradation, or drug clearance starts.

Figure 6 illustrates the time variant drug concentration profiles in the extracellular space (Figure 6a) and reversibly (or irreversibly) electroporated cells (Figure 6b) for different drug permeability. The mass transfer coefficient is directly proportional to the drug permeability (see Eq (3.10)), hence increment in P leads to increment in μ which results in faster decline of drug concentration in the extracellular space from its peak value. On the other hand, in Figure 6b, the contours for increased permeability attain their respective peaks in a shorter time duration in comparison with other contours of reduced permeability. After a certain time (approximately 120 sec), the contours with different permeability get merged with each other because a saturation condition is attained by the cells where drug uptake reaches its maximum limit.

Figure 7 presents the time variant drug concentration profiles in the extracellular region (Figure 7a) and reversibly (or irreversibly) electroporated cells (Figure 7b) for different magnitudes of the electrical field (E). For a low electric field $E = 100$ V cm^{-1}, it is clearly observed from Figure 7a that the drug concentration (C_E) remains unaltered with time. But with the increase in strength of the electric field, the concentration profiles gradually decline from their maximum values. Initiation of drug uptake into the intracellular region depends on μ. And μ depends on the number of pores N_P along with pore radius R_P (see Eq (3.6)). For a low electric field ($E \leq 100$ V cm^{-1}), N_P is very small so as μ. The drug uptake is almost zero for $E \leq 100$ V cm^{-1} and it gets initiated when $E > 100$ V cm^{-1}. So, it is observed that electric field $E > 100$ V cm^{-1} is necessary for the initiation of cell destabilization. Hence, it is calculated in this study that a threshold value ($E > 100$ V cm^{-1}) of the electric field is needed to

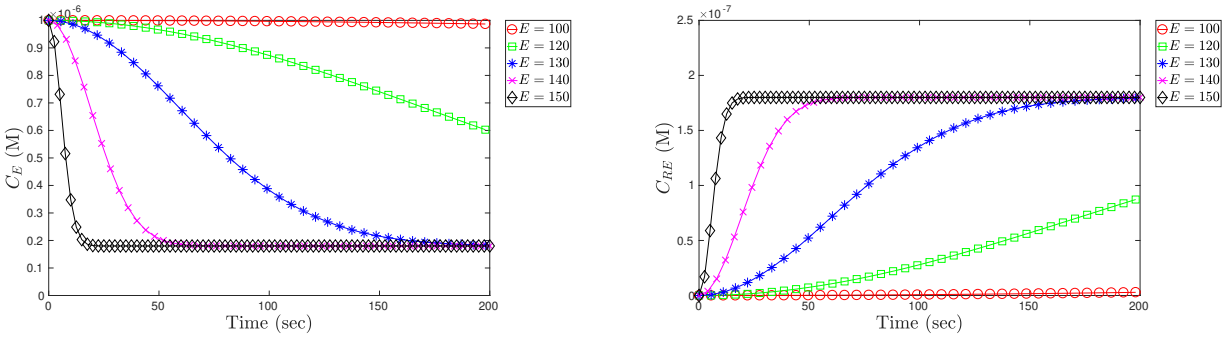

(a) **(b)**

Figure 7. Time variant drug concentration profiles of (a) C_E and (b) C_{RE} (or C_{IRE}) for different E (V cm^{-1}) and $P = 5\times10^{-7}$ m sec^{-1}. The drug concentrations (C_{RE}, C_{IRE}) are analogous to each other as there is no resealing effect and same mass transfer rate in reversibly and irreversibly electroporated cells.

initiate drug uptake into the cells. However, this threshold value may depends on types of drug particles and diseased sites. As time elapses, C_E profiles for higher electric fields decline faster before being merged in comparison with that for lower electric fields. This happens as new pores are formed after the commencement of electroporation. The pore radii are widened with ascending electric field values to allow more drug particles to permeate through the cell membranes. Since the pore density increases with the electrical field, the contours for higher electrical field attain their zenith rapidly due to the faster drug uptake in the cells (Figure 7b).

5.3. Mass transfer after the termination of electroporation

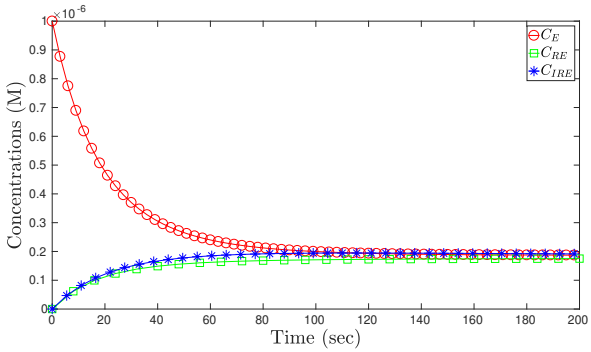

Figure 8. Time variant drug concentration profiles of C_E, C_{RE} and C_{IRE} for $P = 5\times10^{-7}$ m sec^{-1}, E=140 V cm^{-1} and $t_{ep} = 20$ sec.

In this section, it is assumed that mass transfer in the form of drug transport initiates immediately after the completion of the electroporation process. The following graphical portrayals represent various facets of the underlying phenomena when the particular condition mentioned in the Section 3.2 is taken into consideration.

In the case of post electroporation drug transport, Figure 8 represents the time variant drug concentration profiles in the extracellular space, reversibly and irreversibly electroporated cells. From the

figure, it may be observed that the C_E plots gradually decline due to drug diffusion into the intracellular region, whereas the drug concentrations C_{RE} and C_{IRE} increase slowly with time due to drug uptake in the cells. Unlike Figure 5, it can be visualized in Figure 8 that the drug concentration in reversibly electroporated cells is less than the drug concentration in irreversibly electroporated cells. This type of trend could be due to the pore resealing effect that reduces the drug uptake in reversibly electroporated cells after a specific time.

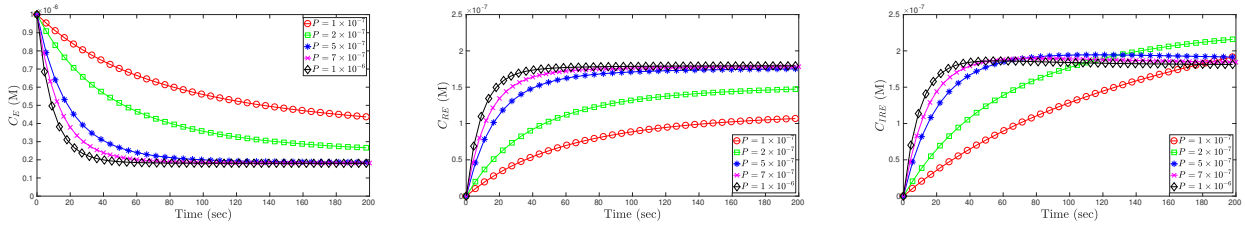

(a) **(b)** **(c)**

Figure 9. Time variant drug concentration profiles of (a) C_E, (b) C_{RE} and (c) C_{IRE} for different P (m sec^{-1}), E=140 V cm^{-1} and t_{ep} = 20 sec.

Figure 9 demonstrates the time-dependent drug concentration profiles in the extracellular space, reversibly and irreversibly electroporated cells, for different values of drug permeability. Figure 9a shows that the concentration graphs for lower permeability take a prolonged time to decay compared to that with higher permeability because increased drug permeability increases the cellular drug uptake. Figure 9b shows that with the increase in drug permeability, the drug uptake consistently enhances. However, one point is noticed in the Figure 9c that prior to a particular time, the C_{IRE} profiles behave similarly to that of C_{RE}. After the specific time, the graphs for lower drug permeability increase more than the maximum limit attained by the graphs of higher drug permeability. This is due to the fact that the initiation of resealing effect restricts the drug uptake by reversibly electroporated cells, and as a result, the surplus drug particles enter into the irreversibly electroporated cells.

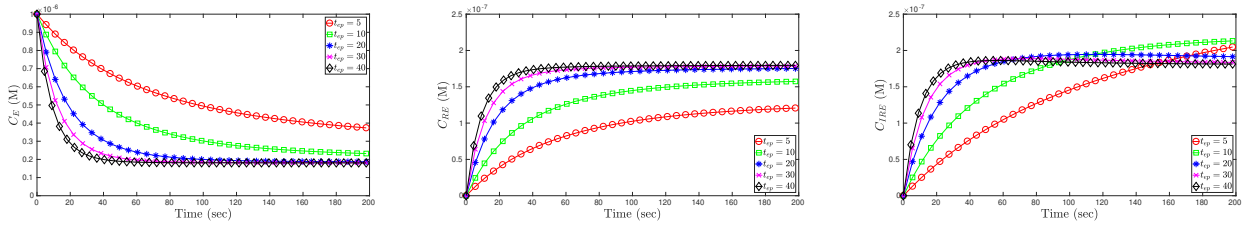

(a) **(b)** **(c)**

Figure 10. Time variant drug concentration profiles of (a) C_E, (b) C_{RE} and (c) C_{IRE} for different t_{ep} (sec), $P = 5 \times 10^{-7}$ m sec^{-1} and $E = 140$ V cm^{-1}. Here, electroporation is performed for different time duration (t_{ep}) before the commencement of drug transfer.

Figure 10 presents the temporal changes of drug concentrations in the extracellular space, reversibly and irreversibly electroporated cells, for different time duration of electroporation. Figure 10a shows that if the time duration increases, the drug uptake gets higher and hence respective concentration C_E declines faster. In both Figure 10b,c, it is observed that if the time span of electroporation is longer, the drug uptake gets higher. This is due to the fact that the application of a long-time electric pulse

creates a large number of pores, and hence permeability of the cell membrane gets increased. It may be observed from Figure 10c that maximum values of the concentration C_{IRE} for the cases $t_{ep} = 5$ sec and $t_{ep} = 10$ sec are more than that of other cases. The reasons are: these pulse periods are so small that resealing effect starts early enough for the reversibly electroporated cells to engulf the surplus drug particles from the extracellular space; a shorter electric pulse leads to a lesser number of pores formation so that the relative resealing effect will have more impact; the resealing effect has changed the mass transfer rate of reversibly electroporated cells but not of irreversibly electroporated cells.

5.4. *Comparison*

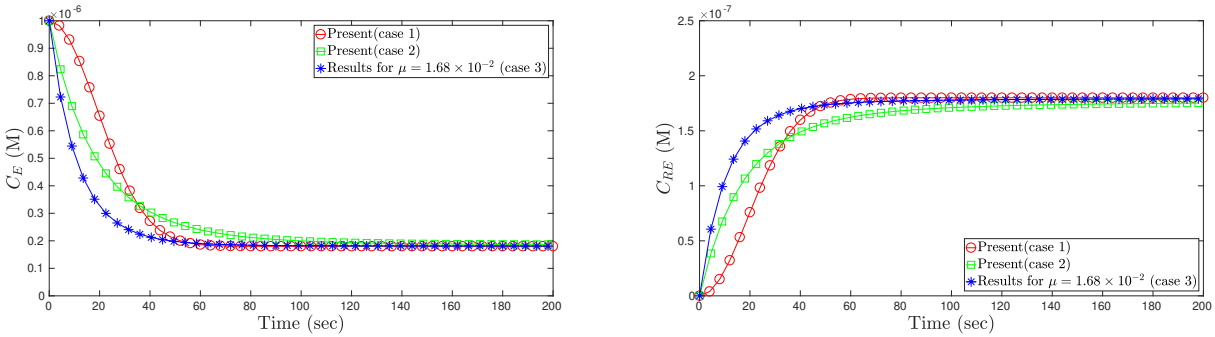

(a) **(b)**

Figure 11. A comparison of drug concentration profiles of (a) C_E and (b) C_{RE} for various cases. Here, in case 1 (present), Equations (3.10)–(3.12) are solved with $P = 5 \times 10^{-7}$ m sec^{-1} and $E = 140$ V cm^{-1}; in case 2 (present), Equations (3.14)–(3.16) are solved with $P = 5 \times 10^{-7}$ m sec^{-1}, $E = 140$ V cm^{-1} and $t_{ep} = 20$ sec; in case 3, Equations (3.14)–(3.16) are solved taking mass transfer coefficient ($\mu = 1.68 \times 10^{-2}$ sec^{-1}) from the model of Kalamiza et al. [24] with $P = 5 \times 10^{-7}$ m sec^{-1}, $E = 140$ V cm^{-1} and $t_{ep} = 20$ sec.

A comparative study is conducted between the results of the present model having variable mass transfer coefficient (cases 1 and 2). Besides, an additional case (case 3) is considered in which a mass transfer coefficient, $\mu = \frac{3D_{eff} \times f_p}{d_m \times r_c}$ is taken from the dual-porosity model of Kalamiza et al. [24] and is substituted in the Eqs (3.14) – (3.16) of our model. In the model of [24], the mass transfer coefficient is formulated using pore surface fraction ratio (f_p), which is well described in the literature [32]. Based on that mass transfer coefficient, the corresponding drug concentrations are calculated and represented graphically as case 3 in Figure 11. The figure represents time variant drug concentration profiles of C_E and C_{RE} for both the cases in the present study along with the case 3 where $\mu = 1.68 \times 10^{-2}$ sec^{-1}(for particular value of f_p [32]). In case 3, a steady decline in C_E (Figure 11a) and a steady increase in C_{RE} (Figure 11b) are noticed as the constant mass transfer coefficient in case 3 is greater than the mass transfer coefficients in cases 1 and 2. In case 1, where electroporation is under way, C_E declines slowly from its maximum concentration in comparison with that of case 2, where the electroporation process is terminated. The reason is that in case 1, new pores are being formed with time during drug transport, and in case 2, the maximum number of pores are already created before drug transport. In Figure 11a, after intersecting at a particular time, the quickly declining curve (i.e., case 2) degrades meagrely in comparison with slowly declining curve (i.e., case 1). This is because by this time, the

resealing effect (case 2) has started influencing the drug transport by slowing down the drug uptake by reversibly electroporated cells. Moreover, due to constant increment in the number of pores for case 1, the resultant drug uptake overcomes that of case 2 after the intersecting point. Figure 11 reveals an important observation that whatever process (case 1 or case 2) is followed to administer the drug in the intracellular domain, the resultant drug uptake is similar. Experimental research on tissue electroporation with respect to the geometry considered in our study is unavailable. Hence, there is little scope to validate our theoretical results with those of experimental ones. However, the graphical representations provided here are analogous to those present in the works of Granot and Rubinsky [11], Kalamiza et al. [24] and Boyd and Becker [26]. This depicts the authenticity of our model.

5.5. *Sensitivity analysis*

In this section, a sensitivity analysis of drug concentrations (C_E, C_{RE}, C_{RE}) with respect to the parameters such as, permeability of drug (P), electric field (E), 'pulse length (t_{ep})' and 'characteristic voltage for electroporation (V_{ep})' for the case 1 is performed and the graphical representation is shown in Figures 12 and 13.

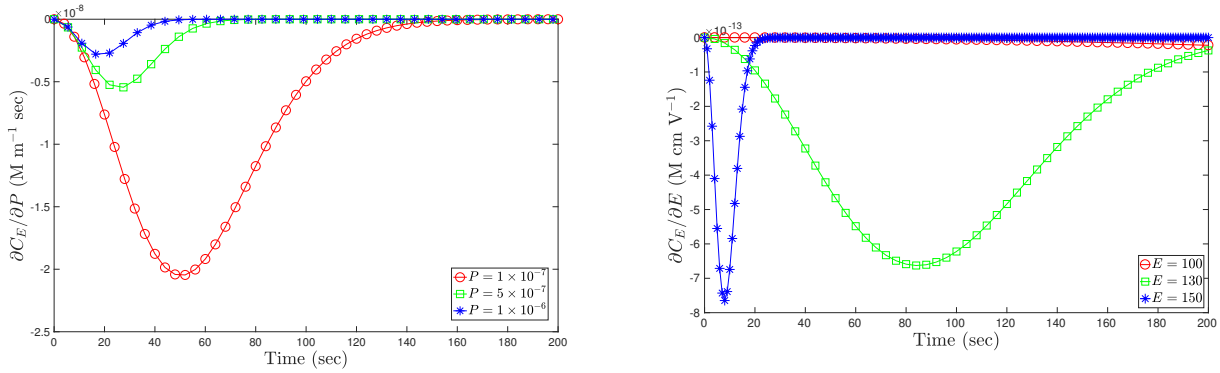

(a) **(b)**

Figure 12. Sensitivity of C_E to the parameters (a) P (m sec^{-1}) and (b) E (V cm^{-1}). From the Eq (4.11), $\frac{\partial C_E}{\partial P}$ at different P and $\frac{\partial C_E}{\partial E}$ at different E are computed and plotted against time.

Figure 12 shows the sensitivity of the drug concentration C_E to the parameters P and E. From Figure 12a, it is observed that deviation in the curve becomes larger with smaller permeability and the deviation approaches to zero near time t = 150 sec. Also, deviations in the curves for higher values of permeability are relatively less. It is clear from Figure 12b that the deviation of the E-variant curve for $E = 100$ V cm^{-1} is almost zero over the entire time. Deviation in the curve for $\frac{\partial C_E}{\partial E}$ increases with the increase in E. In Figure 12, one may notice that the rate of change in the concentration (C_E) with respect to both the parameters is negative due to continuous decrease in mass in the extracellular region.

Figure 13 represents the sensitivity of the drug concentration C_{RE} to the parameters P and E. In Figure 13a, the deviation of the curve for smaller permeability is larger than the curves for higher permeabilities. In Figure 13, it is observed that the rate of change in the concentration (C_{RE}) with respect to both the parameters are positive due to continuous mass uptake in both the intracellular regions. The sensitivity of the drug concentration C_{IRE} is similar to that of C_{RE}. From the above

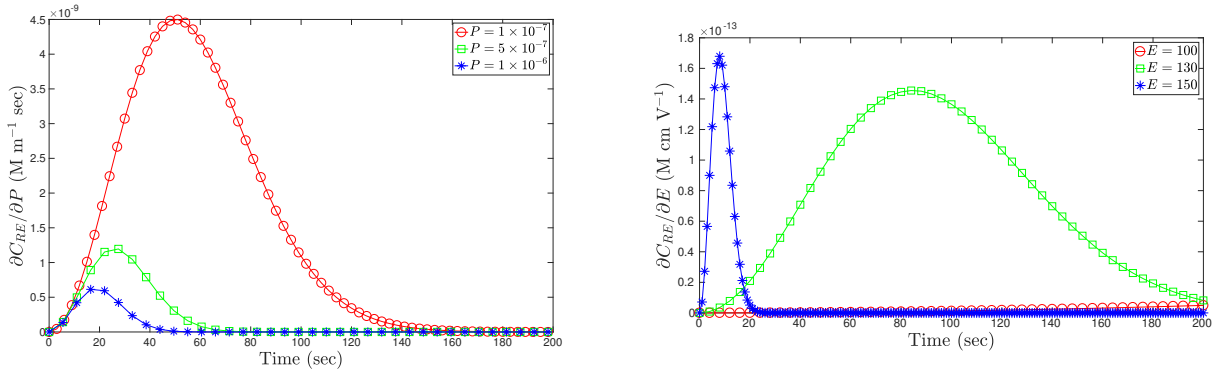

Figure 13. Sensitivity of C_{RE} to the parameters (a) P (m sec^{-1}) and (b) E (V cm^{-1}). From the Eq (4.10), $\frac{\partial C_{RE}}{\partial P}$ at different P and $\frac{\partial C_{RE}}{\partial E}$ at different E are computed and plotted against time.

discussion, it is concluded that the drug concentrations (C_E, C_{RE}, C_{IRE}) are more sensitive to P than that to E.

Sensitivity analysis of drug concentrations with respect to the parameters t_{ep} and V_{ep} are also studied. These parameters are found less sensitive in the resultant drug concentrations (figures are not included). Hence, it is observed from the above sensitivity analysis that the drug concentrations are most sensitive to the drug permeability (P) and least sensitive to characteristic voltage for electroporation (V_{ep}) compared to other parameters.

6. Conclusions

The following observations can be inferred from the outcomes of the present study:

(i) The propounded model is more realistic as vital physical phenomenon i.e., the possibility of transport of drug during electroporation is incorporated.

(ii) Two types of electroporation approaches to drug delivery, like drug delivery during ongoing electroporation and drug delivery just after the termination of electroporation, are simultaneously investigated. It is found that both the approaches give similar results in drug administration to the cells.

(iii) The mass transfer coefficient generally depends on the pore density. The pore density is a function of time during electroporation. In this model, a time-dependent mass transfer coefficient is studied for the first time (to the best of our knowledge).

(iv) The threshold value of the electric field ($E > 100$ V cm^{-1}) to initiate drug uptake in the intracellular regions is the novel outcome of the study.

(v) Through the sensitivity analysis, it is observed that the drug concentrations (C_E, C_{RE}, C_{IRE}) are most sensitive to P and least sensitive to V_{ep}.

(vi) The advocated mathematical model is more accurate. Its authenticity is verified through a comparative study.

Thus, the proposed mathematical model may be used in order to improve drug delivery in the tissue through the electroporation approach. This model could be helpful in various clinical experiments once experimental validations are performed.

Future scope of this study could be as follows:
(i) the effects of drug absorption, metabolism and clearance may be incorporated,
(ii) some assumptions like homogeneous tissue media and uniformly pore distribution could be dropped,
(iii) validation with relevant experimental data, once these are available, may be performed.

Acknowledgments

The first author (Nilay Mondal) acknowledges the support received from the Indian Institute of Technology Guwahati, Assam, India.

Conflict of interest

The authors declare that there is no conflict of interest.

References

1. k K. A. DeBruin, W. Krassowska, Modeling electroporation in a single cell. i. effects of field strength and rest potential, *Biophys. J.*, **77** (1999), 1213–1224.
2. R. V. Davalos, B. Rubinsky, L. M. Mir, Theoretical analysis of the thermal effects during in vivo tissue electroporation, *Bioelectrochemistry*, **61** (2003), 99–107.
3. W. Krassowska, P. D. Filev, Modeling electroporation in a single cell, *Biophys. J.*, **92** (2007), 404–417.
4. T. Kotnik, L. Rems, M. Tarek, D. Miklavčič, Membrane electroporation and electropermeabilization: Mechanisms and models, *Annu. Rev. Biophys.*, **48** (2019), 63–91.
5. J. Dermol-Černe, E. Pirc, D. Miklavčič, Mechanistic view of skin electroporation–models and dosimetry for successful applications: an expert review, *Expert. Opin. Drug. Deliv.*, **17** (2020), 689–704.
6. S. Mahnič-Kalamiza, E. Vorobiev, D. Miklavčič, Electroporation in food processing and biorefinery, *J. Membr. Biol.*, **247** (2014), 1279–1304.
7. T. B. Napotnik, M. Reberšek, P. T. Vernier, B. Mali, D. Miklavčič, Effects of high voltage nanosecond electric pulses on eukaryotic cells (in vitro): A systematic review, *Bioelectrochemistry*, **110** (2016), 1–12.
8. M. Pavlin, D. Miklavčič, Effective conductivity of a suspension of permeabilized cells: A theoretical analysis, *Biophys. J.*, **85** (2003), 719–729.
9. J. Dermol-Černe, D. Miklavčič, From cell to tissue properties-modeling skin electroporation with pore and local transport region formation, *IEEE Trans. Biomed. Eng.*, **65** (2018), 458–468.

10. P. A. Garcia, R. V. Davalos, D. Miklavčič, A numerical investigation of the electric and thermal cell kill distributions in electroporation-based therapies in tissue, *PLoS One*, **9** (2014), 1–12.
11. Y. Granot, B. Rubinsky, Mass transfer model for drug delivery in tissue cells with reversible electroporation, *Int. J. Heat Mass Transf.*, **51** (2008), 5610–5616.
12. M. Pavlin, S. M. Kandu, M. Rebersek, G. Pucihar, F. X. Hart, R. Mag-jareviccacute, et al., Effect of cell electroporation on the conductivity of a cell suspension, *Biophys. J.*, **88** (2005), 4378–4390.
13. R. V. Davalos, L. M. Mir, B. Rubinsky, Tissue ablation with irreversible electroporation, *Ann. Biomed. Eng.*, **33** (2005), 223–231.
14. B. Rubinsky, Irreversible electroporation in medicine, *Technol. Cancer Res. Treat.*, **6** (2007), 255–260.
15. C. Jiang, R. Davalos, J. Bischof, A review of basic to clinical studies of irreversible electroporation therapy, *IEEE Trans. Biomed. Eng.*, **62** (2015), 4–20.
16. D. Miklavčič, G. Serša, E. Brecelj, J. Gehl, D. Soden, G. Bianchi, et al., Electrochemotherapy: technological advancements for efficient electroporation-based treatment of internal tumors, *Med. Biol. Eng. Comput.*, **50** (2012), 1213–25.
17. J. Dermol-Černe, J. Vidmar, J. Ščančar, K. Uršič, G. Serša, D. Miklavčič, Connecting the in vitro and in vivo experiments in electrochemotherapy - a feasibility study modeling cisplatin transport in mouse melanoma using the dual-porosity model, *J. Control. Release*, **286** (2018), 33–45.
18. C. Rosazza, S. H. Meglic, A. Zumbusch, M. P. Rols, D. Miklavčič, Gene electrotransfer: A mechanistic perspective, *Curr. Gene Ther.*, **16** (2016), 98–129.
19. B. Zorec, S. Becker, M. Rebersek, D. Miklavčič, N. Pavselj, Skin electroporation for transdermal drug delivery: The influence of the order of different square wave electric pulses, *Int. J. Pharm.*, **457** (2013), 214–223.
20. S. Čorović, L. M. Mir, D. Miklavčič, In vivo muscle electroporation threshold determination: Realistic numerical models and in vivo experiments, *J. Membr. Biol.*, **245** (2012), 509–520.
21. G. Pucihar, J. Krmelj, M. Reberšek, T. B. Napotnik, D. Miklavčič, Equivalent pulse parameters for electroporation, *IEEE Trans. Biomed. Eng.*, **58** (2011), 3279–3288.
22. S. Satkauskas, M. Bureau, M. Puc, A. Mahfoudi, D. Scherman, D. Miklavčič, et al., Mechnisms of in vivo dna electrotransfer: Respective contributions of cell electropermeabilization and dna electrophoresis, *Mol. Ther.*, **5** (2002), 133–140.
23. J. C. Weaver, Electroporation of biological membranes from multicellular to nano scales, *IEEE Trans. Dielectr. Electr. Insul.*, **10** (2003), 754–768.
24. S. Mahnič-Kalamiza, D. Miklavčič, E. Vorobiev, Dual-porosity model of solute diffusion in biological tissue modified by electroporation, *Biochem. Biophys. Acta. Biomembr.*, **1838** (2014), 1950–1966.
25. S. Mahnič-Kalamiza, D. Miklavčič, E. Vorobiev, Dual-porosity model of mass transport in electroporated biological tissue: Simulations and experimental work for model validation, *Innov. Food Sci. Emerg. Technol.*, **29** (2015), 41–54.
26. B. Boyd, S. Becker, Macroscopic modeling of in vivo drug transport in electroporated tissue, *J. Biomech. Eng.*, **138** (2016), 031008–11.

27. F. Argus, B. Boyd, S. M. Becker, Electroporation of tissue and cells: A three-equation model of drug delivery, *Comput. Biol. Med.*, **84** (2017), 226–234.

28. E. Goldberg, A. Soba, D. Gandía, M. L. Fernández, C. Suárez, Coupled mathematical modeling of cisplatin electroporation, *Bioelectrochemistry*, **140** (2021), 107788.

29. D. Sel, D. Cukjati, D. Batiuskaite, T. Slivnik, L. M. Mir, D. Miklavčič, Sequential finite element model of tissue electropermeabilization, *IEEE Trans. Biomed. Eng.*, **52** (2005), 816–827.

30. R. W. Glaser, S. L. Leikin, L. V. Chernomordik, V. F. Pastushenko, A. I. Sokirko, Reversible electrical breakdown of lipid bilayers: formation and evolution of pores, *Biochem. Biophys. Acta. Biomembr.*, **940** (1988), 275–287.

31. J. C. Neu, W. Krassowska, Asymptotic model of electroporation, *Phys. Rev. E*, **59** (1999), 3471–3482.

32. M. Pavlin, Miklavčič, Theoretical and experimental analysis of conductivity, ion diffusion and molecular transport during cell electroporation-relation between short-lived and long-lived pores, *Bioelectrochemistry*, **74** (2008), 38–46.

AIMS Press